ChemComm

COMMUNICATION

View Article Online
View Journal | View Issue

Cite this: *Chem. Commun.*, 2022, **58**, 5506

Received 11th February 2022,
Accepted 29th March 2022

DOI: 10.1039/d2cc00865c

rsc.li/chemcomm

Dual active sites in a triazine-based covalent organic polymeric framework promoting oxygen reduction reaction†

Tribani Boruah,‡[a] Sabuj Kanti Das,‡[a] Greesh Kumar,‡[a] Saptarsi Mondal[b] and Ramendra Sundar Dey *[a]

A new significant feature of a triazine-based covalent organic polymer electrocatalyst is demonstrated. The metal-free electrocatalyst has dual-active sites, which enable it to entangle oxygen *via* a push–pull interaction that plays a crucial role in promoting the oxygen reduction reaction.

Sustainable energy usage relies on modern energy conversion technologies including water electrolysis enabling hydrogen-fuel evolution and fuel cells/metal–air batteries for generating electricity.[1] In energy storage as well as conversion systems, particularly rechargeable metal–air battery systems or fuel cells, the oxygen reduction reaction (ORR) is the fundamental electrochemical reaction driving their operations.[2] Despite the immense utilization of electrocatalytic materials for ORR, there is a greater emphasis on the development and design of effective electrocatalysts.[3]

Interestingly, to achieve optimal catalytic efficiency, there must be an effective reduction in the energy barriers of catalytic mechanisms as well as an enhancement in the electron transfer rate. Pt-based nanostructures have indeed been regarded as the most active catalysts for ORR,[4] although their high cost and minimal stability have adversely prevented their wide scale commercialization.[5] Consequently, the development of alternative catalysts, such as non-precious metal-based nanomaterials including recently developed metal-free carbon catalysts, has been the focus of considerable attention over the past few decades.[6] Interestingly, some reported class of polymeric framework materials, including metal–organic frameworks (MOFs),[7] porphyrin-based frameworks,[8] and metal-doped covalent organic frameworks (COFs),[9,10] have also demonstrated remarkable performance for ORR. Nevertheless, as a consequence of some major challenges attributed to metal leaching, corrosion, less durability, *etc.*, the organic monomeric precursors linked together *via* strong covalent interaction to form polymeric networks such as covalent organic polymers (COPs), have been considered as new efficient materials in electrocatalysis. Interestingly, the arrangement and adaptability of the constructional building units utilized to develop periodic architectures possessing porous functionality within the 2D or 3D frameworks endow COPs with inherent distinct properties such as high surface area, tunable porosity, sufficient thermal stability and substantial charge mobility.[11] COP-based materials with the strong tailoring of heteroatoms such as nitrogen and extended π-conjugated structural units help in excellent mass transport during the electrocatalytic process. Triazine-based COPs are evolving as existing materials due to their aromatic C=N (triazine unit) and C=NH (imine) linkage and absence of any weak chemical bond that endow the framework with high chemical stability. Abundant nitrogen content in its various forms such as imine and triazine in the π-conjugated carbon networks are not only advantageous for the wettability but also provides enough electroactive surface area.[12] In electrocatalysis, (a) number of active sites, (b) the rate of electron transfer, and (c) stability are the three most important factors considered during the designing of a catalyst. Until now, the chemistry of the active sites on triazine-based COPs for ORR has remained a mystery, opening up a huge scope to explore the origins of their high catalytic activity. Dai *et al.*[13] reported N-induced charge delocalization attributed to the change in the chemisorption mode of O_2 to a side-on (Yeager model) adsorption from the usual end on adsorption (Pauling model) and the parallel diatomic interaction facilitated the ORR through weakening the O–O bond[14] (Scheme 1). Several other researchers have also proposed the mechanistic pathway of ORR *via* the triazine unit, where O_2 prefers to chemisorb on C=N *via* side on mode and forms a conformationally unstable four-membered ring as an intermediate.[15] However, there are no such reports (to the best of our knowledge) that demonstrate O_2 adsorption on dual active sites (triazine and imine units) of the COP/COF/POP-based electrocatalyst.

In this study, we have chosen a model ORR electrocatalyst, Trz-COP (triazine-based COP), with triazine and imine units as dual

[a] *Institute of Nano Science and Technology, Sector- 81, Mohali-140306, Punjab, India. E-mail: rsdey@inst.ac.in*
[b] *Center for Molecular Spectroscopy and Dynamics, Institute of Basic Science (IBS), Seoul 02841, Republic of Korea*

† Electronic supplementary information (ESI) available: Experimental details, TGA, FESEM, additional electrochemical data regarding ORR, DTF calculation. See DOI: https://doi.org/10.1039/d2cc00865c

‡ These authors contributed equally.

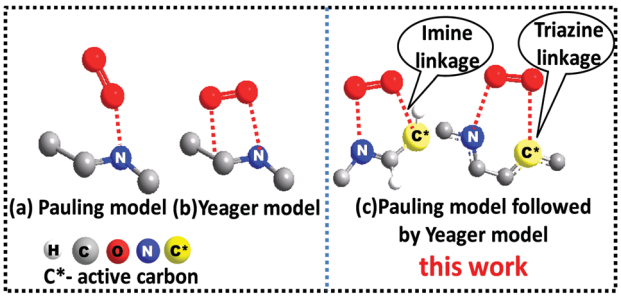

Scheme 1 Diagrammatic representation of existing literature with the present work.

active sites, as presented in Scheme 2. The geometrically favourable interactions of the active sites with O_2, their mechanistic reaction pathway, and the durability for ORR in basic media were explored. Our findings provide valuable insights into the chemisorption of O_2 into the active sites and its electroreduction on catalyst surfaces, which may help in understanding the field and the design of metal-free electrocatalysts for ORR.

The synthesis of the COP material namely Trz-COP using the as-synthesized monomeric precursors, diformylphloroglucinol (DFP) and TAPT (1,3,5-tris-(4-aminophenyl)triazine),[16] is presented in ESI† (^{1}H-NMR of DFP, TAPT and structure of Trz-COP are given in Fig. S1, S2 and S3, ESI† along with their synthesis in Section S1, ESI†). Powder X-ray diffraction (PXRD) study of the Trz-COP catalyst was performed to evaluate the nature of the crystallinity of the polymer matrix (Fig. 1a), where a low intense peak with a 2θ value of 5.6° was observed, indicating a considerably minimal crystallinity of the material. Another broad peak exhibiting a maxima at 26.9° revealed that the Trz-COP is predominantly two-dimensional (2D) in nature. The involvement of angular strain among two monomer units culminates in the polymer's poor crystallinity. The 2D nature of the as-synthesized material was further confirmed by Raman study (Fig. 1b), where the G-band appeared due to the in-plane sp^2 hybridization present in the organic polymeric network and the presence of D-band inferred the out-of-plane vibrations attributed to the presence of defects in the framework.[17] The morphology of the

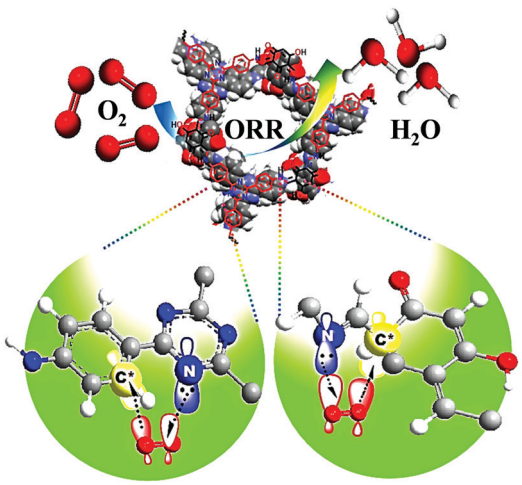

Scheme 2 Schematic representation of dual active site of Trz-COP.

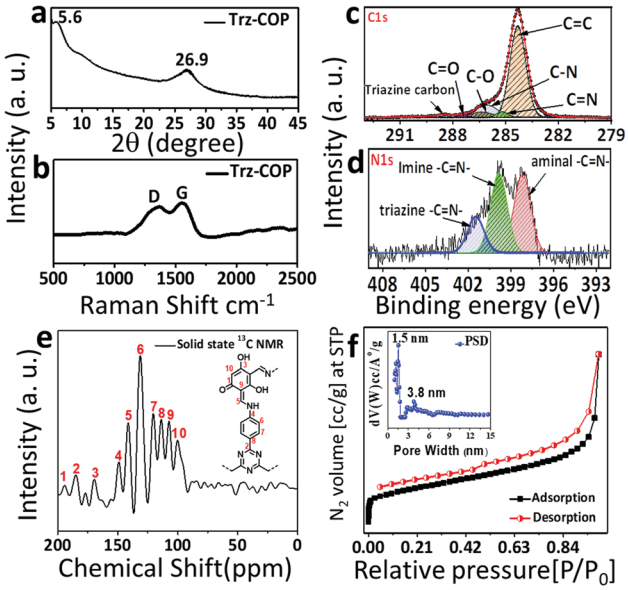

Fig. 1 (a) PXRD pattern, (b) Raman spectra, (c and d) XPS spectra of C 1s and N 1s atoms, (e) ^{13}C CP MAS NMR spectrum, (f) N_2 adsorption/desorption isotherm with pore size distribution (inset) of Trz-COP.

as-synthesized polymeric network was examined *via* the field emission scanning electron microscopy (FE-SEM) technique. FE-SEM images display agglomerated particles through a self-assembled approach. In addition, we collected the FESEM images of a base-treated (0.5 M KOH for 3 days) sample (Fig. S4, ESI†), which displayed the same morphology as that of the as-synthesized material, which confirms the morphological stability of the material. The chemical orientation of C-atoms and the bonding connectivity were further confirmed by XPS, FTIR and solid state ^{13}C-NMR analysis. In the FTIR spectrum, a broad peak appeared at 3412 cm^{-1} (two merged peaks) along with two peaks at 1510 and 1413 cm^{-1}, which indicate the stretching as well as bending vibration bands of –N–H and –O–H functionalities, respectively (Fig. S4c and Table S3, ESI†). The deconvoluted C 1s XPS spectra shows peaks at 288.4, 287.5, 286.5, 286.03, 285.2, 284.3 eV, suggesting the presence of –C═N–(triazine), –C═O–, C–O, C–N, –C═N and, C═C functionalities, respectively. Similarly, deconvoluted N 1s spectra also depicted peaks at 399.9 (triazine), 399.16 (imine) and 398.11 eV (aminal), clearly demonstrating the presence of three different types of N-functionalities (Fig. 1c and d, Fig. S5, Tables S1 and S2, ESI†).[18] The ^{13}C MAS NMR (magic angle spinning nuclear magnetic resonance) spectrum (Fig. 1e) displays peaks at 194.3 ppm and 185 ppm, confirming the presence of a carbonyl carbon (1) and carbon (2) in the triazine ring, respectively. The signals at 169.5 ppm and 149.2 ppm (sharp peaks) correspond to the C-atoms attached to the hydroxyl functional unit (3) and sp^2 hybridized carbon (4) of the benzene moieties present adjacent to –NH/–C═N functionality. A sharp resonance signal at 141.3 ppm indicates the presence of imine as well as aminal-linked carbon atoms (5). In ^{13}C-NMR, the appearance of strong resonance peaks around 131.2, 120.3, 113.8, 107.2 and 100.2 ppm indicate the existences of different aromatic C-atoms present in the Trz-COP polymeric network (C atoms marked as 6, 7, 8, 9 and 10, respectively). Before investigating the catalytic

efficiency as well as surface area analysis, the thermal stability of a material must be examined. The thermogravimetric analysis (TGA) illustrates that the molecular architecture of the Trz-COP porous polymeric matrix is stable up to 400 °C (Fig. S6, ESI†). Furthermore, N_2 adsorption/desorption isotherms (Fig. 1f) were categorized as type I, followed by type IV isotherm with a hysteresis loop and a sharp increase at the high-pressure region, which indicate the presence of microporosity, mesoporosity and interparticle porosity, respectively. The specific surface area and the total pore volume were obtained to be 715 $m^2\ g^{-1}$ and 1.27 cc g^{-1} at P/P_0 of 0.9932, respectively, with a pore size distribution of 1.5 nm and 3.8 nm (inset Fig. 1f). Therefore, the high SSA and various types of porosity are actually responsible for the high electrocatalytic activity of the material. In addition, the PXRD and FTIR of the imine-based TPA-COF are provided in Fig. S7 in ESI.†

To investigate the electrochemical activity of Trz-COP towards ORR, cyclic voltammetry (CV) was performed in Ar- and O_2-saturated (0.1 M KOH) electrolyte solutions at 10 mV s^{-1} scan rate. The CV displayed no peak in Ar-saturated environment, whereas the appearance of a sharp cathodic peak in the O_2-saturated electrolyte reflected the catalytic efficiency of Trz-COP towards ORR (Fig. S8, ESI†). A hydrodynamic linear sweep voltammetry (LSV) test was performed with our catalyst Trz-COP and the commercially available state-of-the-art Pt/C, using the rotating disk electrode (RDE) technique at 1600 rpm (Fig. S9, ESI†). The acquired potentials were standardized to a reversible-hydrogen electrode (RHE) using the formula, as described in eqn (S1) (Section S1, ESI†). The Trz-COP delivered a half-wave potential ($E_{1/2}$) of 0.73 V (*versus* RHE) and a larger limiting current density (J_L) of 5.2 mA cm^{-2}. Notably, the performance of the catalyst was comparable with that of the commercially available Pt/C (20 wt%) catalyst and better than that of the control samples including respective monomeric units (DFP, triazine linkage containing TAPT) as well as imine only containing TPA-COF (Fig. 2a, Fig. S9 ESI†). The significant ORR performance of this metal free catalyst was further evaluated by electrochemical impedance spectroscopy (Fig. S10, ESI†), which displayed lower R_s and R_{ct} values implying its faster ion diffusion rate and faster electron transport kinetics. An increase in the current density in the LSV curve for Trz-COP was noticeable with an increase in rotation speeds from 625 to 4900 rpm, implying higher mass transportation on the catalyst surface (Fig. S11, ESI†) Subsequently, the linearity of the Koutecky–Levich (K–L) plots generated from LSV curves at various potentials, and at different rotation speeds denoted the first order kinetics of ORR (Fig. 2b). The rotating ring disk electrode (RRDE) technique was rendered to calculate the no. of electrons and % H_2O_2 (Section S1, eqn (S5), (S6), Fig. S12, ESI†). At a varied potential range, the no. of electrons for ORR was consistent with a value of ~3.54 (inset Fig. 2b), defining an almost 4-electron associated mechanism. Over the oxygen reduction potential range, a minimum of 23% H_2O_2 production (inset Fig. 2b), indicated that the entire ORR approach with the Trz-COP catalyst substantially resembled overall $4e^-$ route, taking a path from O_2 to OH^- than to OH^-_2. Further, the reaction kinetics were also confirmed *via* the Tafel-slope interpretation of Trz-COP with Pt/C as the benchmark catalyst, where, a Tafel-slope of 70 mV dec^{-1} for Trz-COP was comparable to the commercialized Pt/C (73 mV dec^{-1}) and lower than those of the respective monomeric units (DFP = 143 mV dec^{-1},

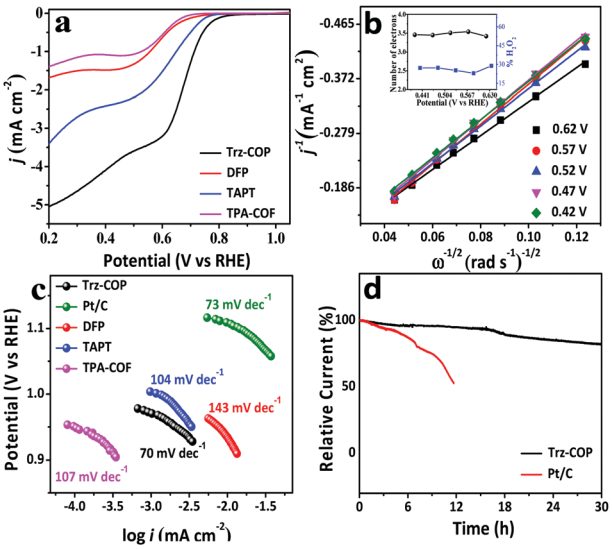

Fig. 2 ORR electrochemical performance of Trz-COP and controlled samples. (a) LSV polarization plots of Trz-COP, DFP, TAPT, TPA-COF. (b) Koutecky–Levich (K–L) plots at various potentials, inset (b)-number of electrons (n) and % H_2O_2. (c) Corresponding Tafel plot of Trz-COP, Pt/C catalyst, monomeric units (DFP, TAPT) rpm and TPA-COF. (d) Stability of Trz-COP and Pt/C using chronoamperometry technique.

TAPT = 104 mV dec^{-1}) (Fig. 2c). Thus, the lower Tafel-slope implies a low over potential ORR for the material promoting a faster kinetic behavior in the electro-catalytic reaction, which might be attributed to the coexistence of dual active sites along with the presence of two types of pores (meso and micro-porous). In addition, the stability studies of the catalyst in an O_2-saturated basic medium displayed a retention of 87% of the initial current density after 24 h better than the commercial Pt/C catalyst (Fig. 2d), which might be due to the presence of a strong extended π-conjugated covalent network within the metal-free Trz-COP electrocatalyst. The LSV curve performed before and after stability measurements showed only a 15 mV shift in the half wave potential after 24 h (Fig. S13, ESI†). In fact the catalyst was found to be tolerant to methanol cross-over effects, as observed from the chronoamperometry and CV curves (with and without 1 M CH_3OH to an O_2-saturated basic electrolyte solution) in Fig. S14, S15, S16 in ESI,† better than the commercially available Pt/C catalyst. Furthermore, to confirm the integrity of the material, we have performed post-stability characterization, as provided in the ESI† as Fig. S17 and S5.

A vivid density functional theory (DFT) study was performed in order to acquire atomic level insight into the interaction of the underlying nanostructures of Trz-COP and their catalytic performance as well as to better comprehend the dual catalytically active center in the catalyst contributing towards the O_2 reduction pathway on the electrode surface (Fig. S18, ESI†). As a result of our calculations, herein, the ORR is promoted *via* both the adsorption and desorption phenomena, preferring the adsorbed O_2 molecules to interact with carbon and nitrogen atoms that are located in a suitable orientation. From the DFT calculations, the complexation energy of A1 (−5.24 kcal mol^{-1}) and A2 (−1.87 kcal mol^{-1}) (Fig. S19, S20, Table S4 in ESI†) suggest the preferred O_2 adsorption sites, leading to the bond elongation of the O_2 molecule (0.031 Å) (detailed

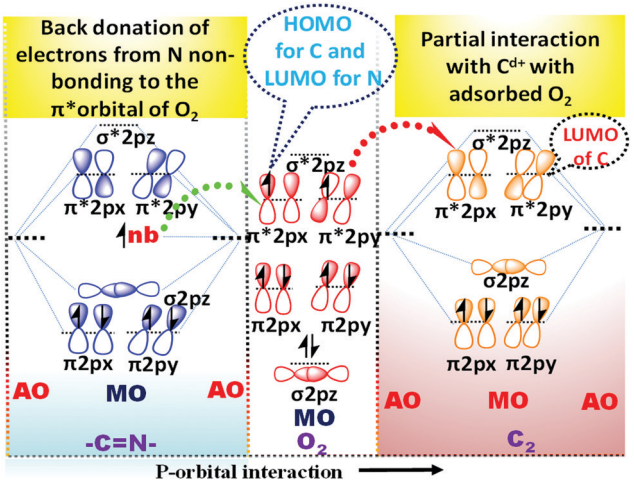

Fig. 3 Diagrammatic representation of molecular orbital interaction between C*, N, O_2.

explanation in Section S2 and S3, ESI†). Owing to the presence of electronegative N atoms in our framework, charge re-distribution triggered the bond polarizability of the constituent atoms. This led to a partial positive charge over the active C atom (C*), which enabled the reactant O_2 molecules to be adsorbed on the C*-site following the Pauling model. A partial O═O bond polarization occurred, wherein the nitrogen lone pairs from triazine-N and imine-N respectively interacted with the partially $O^{\delta+}$ end of the absorbed O_2 molecule following the Yeager model forming orientationally favored 6 and 5 membered rings as per our proposed mechanism (Fig. S21, ESI†). This end-on followed by the side-on adsorption of O_2 facilitated the O_2 bond dissociation yielding the 4 e^- product OH^-. To better understand the feasibility of our proposed mechanism, effective overlapping of the HOMO–LUMO (HOMO = highest occupied molecular orbital, LUMO = lowest unoccupied molecular orbital) groups between the C*, N and O_2 were framed. Presumably, a push–pull interaction operated between C*, N and O atoms, which is explained by a correlation molecular orbital diagram (Fig. 3). We have interpreted that first there is a partial transfer of electrons from the antibonding orbital of the adsorbed O_2 molecule (HOMO) into the antibonding orbital (LUMO) of the partially positively charged carbon atom (C_2). Simultaneously, the back-donation of electrons occurs from the non-bonding orbital of nitrogen in –C═N (HOMO) into the antibonding orbital of oxygen (LUMO), which facilitates the dissociation of the oxygen double bond, promoting ORR.[19] To complement this interaction, we performed a DFT analysis of the Trz-COP electrocatalyst, which is explained in detail in Sections S2 and S3 in ESI.† Consequently, the Trz-COP electrode effectively generated metal-free active sites for the electrochemical reduction of O_2 *via* charge redistribution. So, the appropriate geometrical arrangement of Trz-COP and the preferable type of oxygen adsorption on it assisted in the enhanced activity of the Trz-COP electrocatalyst towards the ORR.

In summary, a 2D extended π-conjugated covalent organic polymer network was synthesised, containing dual active sites with two types of porosity that accelerated the ORR, showing moderately high half wave potential with high stability and methanol tolerance. Further experimental findings were supported by a DFT study, illustrating the weak non-covalent push and pull interaction between adsorbed O_2 and the catalytic surface through the formation of 5 and 6 membered ring intermediates, displaying dual active sites by following both Pauling and Yeager models.

TB thanks SERB/CRG, SKD thanks INST and GK thanks UGC for fellowship, RSD acknowledges DST SERB (CRG/2020/005683) for financial support.

Conflicts of interest

There are no conflicts to declare.

Notes and references

1 F. Vilela, K. Zhang and M. Antonietti, *Energy Environ. Sci.*, 2012, **5**, 7819–7832.
2 F. Cheng and J. Chen, *Chem. Soc. Rev.*, 2012, **41**, 2172.
3 D.-W. Wang and D. Su, *Energy Environ. Sci.*, 2014, **7**, 576–591.
4 Y. Nie, L. Li and Z. Wei, *Chem. Commun.*, 2021, **57**, 12898–12913.
5 L. Fan, Z. Tu and S. H. Chan, *Energy Rep.*, 2021, **7**, 8421–8446.
6 C. Hu, Y. Xiao, Y. Zou and L. Dai, *Electrochem. Energy Rev.*, 2018, **1**, 84–112.
7 M. O. Cichocka, Z. Liang, D. Feng, S. Back, S. Siahrostami, X. Wang, L. Samperisi, Y. Sun, H. Xu, N. Hedin, H. Zheng, X. Zou, H.-C. Zhou and Z. Huang, *J. Am. Chem. Soc.*, 2020, **142**, 15386–15395.
8 Z. Liang, H.-Y. Wang, H. Zheng, W. Zhang and R. Cao, *Chem. Soc. Rev.*, 2021, **50**, 2540–2581.
9 T. Hosokawa, M. Tsuji, K. Tsuchida, K. Iwase, T. Harada, S. Nakanishi and K. Kamiya, *J. Mater. Chem. A*, 2021, **9**, 11073–11080.
10 M. Das, A. Biswas and R. S. Dey, *Chem. Commun.*, 2022, **58**, 1934–1937.
11 D.-H. Yang, Y. Tao, X. Ding and B.-H. Han, *Chem. Soc. Rev.*, 2022, **51**, 761–791.
12 M. Liu, L. Guo, S. Jin and B. Tan, *J. Mater. Chem. A*, 2019, **7**, 5153–5172.
13 G. Kuanping, D. Feng, X. Zhenhai, D. Michael and D. Liming, *Science*, 2009, **323**, 760–764.
14 Z. Shi, J. Zhang, Z.-S. Liu, H. Wang and D. P. Wilkinson, *Electrochim. Acta*, 2006, **51**, 1905–1916.
15 Z. Xiang, D. Cao, L. Huang, J. Shui, M. Wang and L. Dai, *Adv. Mater.*, 2014, **26**, 3315–3320.
16 P. Bhanja, S. K. Das, K. Bhunia, D. Pradhan, T. Hayashi, Y. Hijikata, S. Irle and A. Bhaumik, *ACS Sustainable Chem. Eng.*, 2018, **6**, 202–209.
17 N. Kamboj, T. Purkait, M. Das, S. Sarkar, K. S. Hazra and R. S. Dey, *Energy Environ. Sci.*, 2019, **12**, 2507–2517.
18 W.-R. Cui, C.-R. Zhang, W. Jiang, F.-F. Li, R.-P. Liang, J. Liu and J.-D. Qiu, *Nat. Commun.*, 2020, **11**, 436.
19 L. Yang, S. Jiang, Y. Zhao, L. Zhu, S. Chen, X. Wang, Q. Wu, J. Ma, Y. Ma and Z. Hu, *Angew. Chem., Int. Ed.*, 2011, **50**, 7132–7135.